Journal of Organometallic Chemistry xxx (2014) 1–12

Contents lists available at ScienceDirect

Journal of Organometallic Chemistry

journal homepage: www.elsevier.com/locate/jorganchem

Spectroelectrochemical study of complexes $[Mo(CO)_2(\eta^3\text{-allyl})(\alpha\text{-diimine})(NCS)]$ (α-diimine = bis(2,6-dimethylphenyl)-acenaphthenequinonediimine and 2,2′-bipyridine) exhibiting different molecular structure and redox reactivity

Joanne Tory, Gaël Gobaille-Shaw, Ann M. Chippindale, František Hartl*

Department of Chemistry, University of Reading, Whiteknights, Reading RG6 6AD, UK

ARTICLE INFO

Article history:
Received 16 November 2013
Received in revised form
12 January 2014
Accepted 16 January 2014

Dedicated to Professor Maria José Calhorda on the occasion of her 65th birthday.

Keywords:
Molybdenum
Allyl ligand
α-Diimine ligand
X-ray analysis
Spectroelectrochemistry
Carbon dioxide

ABSTRACT

The redox properties and reactivity of $[Mo(CO)_2(\eta^3\text{-allyl})(\alpha\text{-diimine})(NCS)]$ (α-diimine = bis(2,6-dimethylphenyl)-acenaphthenequinonediimine (2,6-xylyl-BIAN) and 2,2′-bipyridine (bpy)) were studied using cyclic voltammetry and IR/UV–Vis spectroelectrochemistry. $[Mo(CO)_2(\eta^3\text{-allyl})(2,6\text{-xylyl-BIAN})(NCS)]$ was shown by X-ray crystallography to have an asymmetric (B-type) conformation. The extended aromatic system of the strong π-acceptor 2,6-xylyl-BIAN ligand stabilises the primary $1e^-$-reduced radical anion, $[Mo(CO)_2(\eta^3\text{-allyl})(2,6\text{-xylyl-BIAN}^{\bullet-})(NCS)]^-$, that can be reduced further to give the solvento anion $[Mo(CO)_2(\eta^3\text{-allyl})(2,6\text{-xylyl-BIAN})(THF)]^-$. The initial reduction of $[Mo(CO)_2(\eta^3\text{-allyl})(bpy)(NCS)]$ in THF at ambient temperature results in the formation of $[Mo(CO)_2(\eta^3\text{-allyl})(bpy)]_2$ by reaction of the remaining parent complex with $[Mo(CO)_2(\eta^3\text{-allyl})(bpy)]^-$ produced by dissociation of NCS^- from $[Mo(CO)_2(\eta^3\text{-allyl})(bpy^{\bullet-})(NCS)]^-$. Further reduction of the dimer $[Mo(CO)_2(\eta^3\text{-allyl})(bpy)]_2$ restores $[Mo(CO)_2(\eta^3\text{-allyl})(bpy)]^-$. In PrCN at 183 K, $[Mo(CO)_2(\eta^3\text{-allyl})(2,6\text{-xylyl-BIAN}^{\bullet-})(NCS)]^-$ converts slowly to $2e^-$-reduced $[Mo(CO)_2(\eta^3\text{-allyl})(2,6\text{-xylyl-BIAN})(PrCN)]^-$ and free NCS^-. At room temperature, the reduction path in PrCN involves mainly the dimer $[Mo(CO)_2(\eta^3\text{-allyl})(bpy)]_2$; however, the detailed course of the reduction within the spectroelectrochemical cell is complicated and involves a mixture of several unassigned products. Finally, it has been shown that the five-coordinate anion $[Mo(CO)_2(\eta^3\text{-allyl})(bpy)]^-$ promotes in THF reduction of CO_2 to CO and formate via the formation of the intermediate $[Mo(CO)_2(\eta^3\text{-allyl})(bpy)(O_2CH)]$ and its subsequent reduction.

1. Introduction

There is significant and sustained interest in the catalytic reduction of CO_2 to materials that may be used in fuel cells, as chemical fuel sources, or as a feedstock for organic synthesis. A number of different transition-metal complexes have been identified as potential redox catalysts for CO_2 reduction, including macrocyclic complexes, phosphine complexes, and complexes with α-diimine ligands [1–5]. The Group 7 complexes, $[Re(CO)_3(bpy)Cl]$ and related species, are known to act as catalyst precursors for efficient electrochemical and photochemical CO_2 reduction, with the active catalysts being five-coordinate, $1e^-$ reduced radical or $2e^-$ reduced anionic species [6–8]. The manganese analogue, $[Mn(CO)_3(bpy)Br]$, containing the cheaper and more abundant first row transition-metal centre, has recently been shown to act as an electrochemical catalyst for the conversion of CO_2 to CO in the presence of small concentrations of acid, with an overall $2e^-$ reduction to $[Mn(CO)_3(bpy)]^-$ [9,10]. Much less attention in this regard has been devoted so far to Group 6 metal carbonyl α-diimine complexes. Only recently we have encountered similar catalytic activity towards CO_2 reduction exhibited by the structurally related $2e^-$ reduced complex $[Mo(CO)_3(bpy)]^{2-}$ [11].

Another family of Group 6 metal carbonyls, of the type $[Mo^{II}(CO)_2(\eta^3\text{-allyl})(L\cap L)X]$ ($L\cap L$ = chelating bidentate ligand, X = anionic monodentate ligand), are known to have variable stereochemistry. These complexes usually adopt either a symmetric structure with both $L\cap L$ donor atoms trans to equatorial carbonyl ligands (type A), or an asymmetric structure where the η^3-allyl ligand and a carbonyl ligand are trans to $L\cap L$ (type B) as seen in Chart 1 [12–14]. Trans-dicarbonyl isomers, although rare, are also observed [15]. For the cis-dicarbonyl complexes the less common B-type structure occurs particularly when $L\cap L$ is a diphosphine or a

* Corresponding author.
E-mail address: f.hartl@reading.ac.uk (F. Hartl).

0022-328X/$ – see front matter © 2014 Elsevier B.V. All rights reserved.
http://dx.doi.org/10.1016/j.jorganchem.2014.01.015

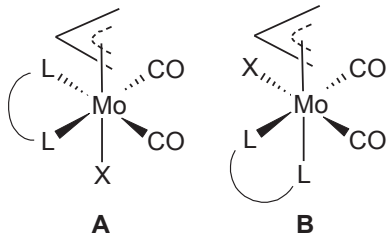

Chart 1. The "A" and "B" type structures observed for $[Mo(CO)_2(\eta^3\text{-allyl})(L\cap L)X]$ complexes.

non-rigid bidentate ligand; although, many exceptions are known in the literature [13–15], and the nature of the X ligand also affects the conformation. For both the A and B structural types, the axial η^3-allyl ligand adopts the orientation where the open face is over the two carbonyl groups. Quantum mechanical (DFT, EHMO) calculations have shown that this is the most stable arrangement for both isomers [13,16].

There are few electrochemical studies of $[Mo(CO)_2(\eta^3\text{-allyl})(L\cap L)X]$ complexes reported in the literature, and these only consider their anodic behaviour. A single one-electron reversible oxidation is observed at 0.5–0.7 V vs. SCE for a range of $[Mo(CO)_2(\eta^3\text{-allyl})(L\cap L)X]$ ($L\cap L$ = bpy, $Ph_2PCH_2PPh_2$, $Ph_2PCH_2CH_2PPh_2$, $Ph_2AsCH_2CH_2AsPh_2$; X = Cl, O_2CCF_3) complexes in dichloromethane (DCM), resulting in the formation of the $[Mo(CO)_2(\eta^3\text{-allyl})(L\cap L)X]^+$ cation with retention of the stereochemistry. Substitution of the chelating bidentate $L\cap L$ ligand for a pair of monodentate ligands results in an electrochemically and chemically irreversible oxidation process [17]. Oxidation of complexes with strongly π-accepting diphosphine and diarsine chelating ligands is less reversible at slower scan rates than for complexes containing α-diimine ligands such as bpy, 1,10-phenanthroline (phen) and *N*,*N*′-di-*tert*butyl-1,4-diazabuta-1,3-diene (^{t}Bu-DAB). IR spectroelectrochemistry of $[Mo(CO)_2(\eta^3\text{-allyl})(L\cap L)X]$ usually shows the two ν(CO) bands shifted to higher frequencies by more than 100 cm^{-1} upon oxidation, in line with the dominant metal localization of the HOMO [18].

In this paper, the electrochemical behaviour of $[Mo(CO)_2(\eta^3\text{-allyl})(bpy)(NCS)]$, together with its ability to catalyse the reduction of CO_2, are investigated. To date, no studies of the reduction of complexes of the type $[Mo(CO)_2(\eta^3\text{-allyl})(\alpha\text{-diimine})X]$ have been reported, and predictions of the electrochemical mechanisms can only be based on comparisons with similar complexes such as $[M(CO)_3(\alpha\text{-diimine})X]$ (M = Mn, Re) [7,9,19,20]. The related complex, $[Mo(CO)_2(\eta^3\text{-allyl})(2,6\text{-xylyl-BIAN})(NCS)]$ (2,6-xylyl-BIAN = bis(2,6-dimethylphenyl)-acenaphthenequinonediimine, Chart 2), is used for comparative electrochemical studies as the extended π-delocalised aromatic system of the 2,6-xylyl-BIAN ligand [21] can stabilise the reduction products.

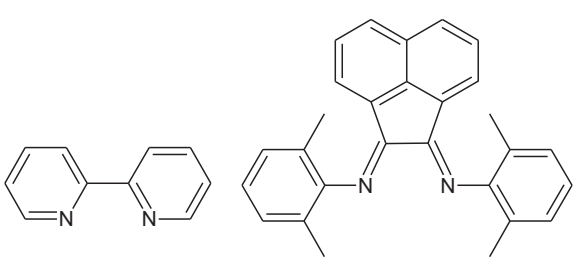

Chart 2. The ligands 2,2′-bipyridine (bpy, left) and bis(2,6-dimethylphenyl)-acenaphthenequinonediimine (2,6-xylyl-BIAN, right).

2. Experimental

2.1. Materials

All solvents were freshly distilled under a nitrogen atmosphere. Tetrahydrofuran (THF) and hexane were distilled from benzophenone/sodium, acetonitrile (MeCN) over P_2O_5, and butyronitrile (PrCN) and dichloromethane (DCM) over CaH_2. The supporting electrolyte, Bu_4NPF_6 (TBAH, Aldrich), was recrystallised twice from absolute ethanol and dried under vacuum. $[Mo(CO)_2(\eta^3\text{-allyl})(MeCN)_2(NCS)]$ [22] and 2,6-xylyl-BIAN [21] were prepared according to literature procedures. The previously reported complex, $[Mo(\eta^3\text{-allyl})(CO)_2(bpy)(NCS)]$ [23,24], was prepared for the purpose of this comparative study by the facile thermal substitution reaction of $[Mo(\eta^3\text{-allyl})(CO)_2(MeCN)_2(NCS)]$ with 2,2′-bipyridine and identified by its IR spectrum in CH_2Cl_2: ν(CO) at 1950, 1867 cm^{-1}, ν(CN): 2079 cm^{-1}. Its purity was further confirmed by ^{1}H NMR spectroscopy. Elemental analysis was carried out by MEDAC Ltd. ^{1}H NMR spectra were recorded on a Bruker NanoBay spectrometer. All electrochemical and spectroelectrochemical measurements were carried out under an inert atmosphere of dry N_2 or argon, using Schlenk techniques. Solutions were saturated with CO_2 at normal pressure by bubbling it through a frit.

2.1.1. $[Mo(CO)_2(\eta^3\text{-allyl})(2,6\text{-xylyl-BIAN})(NCS)]$

A solution of 2,6-xylyl-BIAN (0.59 g, 1.5 mmol) in DCM (15 mL) was added to a solution of $[Mo(\eta^3\text{-allyl})(CO)_2(NCS)(MeCN)_2]$ (0.5 g, 1.5 mmol) in DCM (15 mL) under an atmosphere of dry argon. The mixture was heated under reflux for 3 h, and then reduced to half its volume and the solid complex precipitated with hexane (10 mL). The dark-green precipitate was filtered and washed with cold hexane under inert conditions. Yield: 80–90%. The complex was crystallised from DCM/hexane.

IR in CH_2Cl_2 ν(CO): 1946, 1871 cm^{-1}, ν(CN): 2075 cm^{-1}. UV–vis in CH_2Cl_2 (λ_{max}): 219, 241, 324, 338, 370 and 725 nm. ^{1}H NMR (400 MHz, CD_2Cl_2) δ_{ppm}: 7.96 (2H, d, 2,6-xylyl-BIAN), 7.35 (8H, m, 2,6-xylyl-BIAN), 6.41 (2H, d, 2,6-xylyl-BIAN), 3.48 (1H, m, H_{meso}), 3.12 (2H, br, H_{syn}), 2.36 (6H, s, 2,6-xylyl-BIAN), 2.22 (6H, s, 2,6-xylyl-BIAN), 1.27 (2H, d, H_{anti}). Anal. Calc. for $C_{34}H_{29}MoN_3O_2S(CH_2Cl_2)_{0.5}$ (682.09): C, 57.19; H, 4.17; N, 5.80%. Found: C, 57.21; H, 4.40; N, 5.62%.

2.2. X-ray structure determination

A crystal of $[Mo^{II}(CO)_2(\eta^3\text{-allyl})(2,6\text{-xylyl-BIAN})(NCS)]$ was mounted under Paratone-N oil and flash cooled to 150 K in a stream of nitrogen in an Oxford Cryostream cooler. Single-crystal X-ray intensity data (Table 1) were collected using an Agilent Gemini S Ultra diffractometer (Cu Kα radiation (λ = 1.54180 Å)).

The data were reduced within the CrysAlisPro software [25]. The structure was solved using the program Superflip [26] and all non-hydrogen atoms located. Least-squares refinements on *F* were carried out using the *CRYSTALS* suite of programs [27]. The non-hydrogen atoms were refined anisotropically. Each hydrogen atom of the 2,6-xylyl-BIAN and allyl ligands was placed geometrically with a C–H distance of 0.95 Å and a U_{iso} of 1.2 times the value of U_{eq} of the parent C atom. The positions of the hydrogen atoms were then refined with riding constraints. There are two molecules of $[Mo(CO)_2(\eta^3\text{-}C_3H_5)(NCS)(C_{27}N_2H_{24})]$ in the asymmetric unit, which are mirror images of each other, which give rise to four molecules in the unit cell. The unit cell also contains two large solvent-accessible voids, each with a volume of 129 Å^3, located at (0.480, 0.519, 0.785) and (0.520, 0.481, 0.215). Each of these voids corresponds to a disordered molecule of dichloromethane, which could not be modelled as discrete atomic sites. PLATON SQUEEZE

Table 1
Crystallographic data for [$Mo^{II}(CO)_2(\eta^3$-allyl)(2,6-xylyl-BIAN)(NCS)].

Formula	$(C_{34}H_{29}MoN_3O_2S)(CH_2Cl_2)_{0.5}$
M_r	682.088
Crystal system	Triclinic
Space group	*P*-1
Z	4
a/Å	11.0821(4)
b/Å	16.9712(6)
c/Å	17.9778(4)
α/°	101.499(3)
β/°	103.627(3)
γ/°	99.944(3)
V/Å^3	3133.24(19)
D_{calc}/g cm^{-3}	1.446
Crystal habit	Green plate
Crystal dimensions/mm	0.1 × 0.05 × 0.04
Radiation	Cu K_α (1.54080 Å)
T/K	150
μ/mm^{-1}	5.114
R(*F*), *Rw*(*F*)	3.55, 3.49

software enabled the contribution to diffraction of these disordered solvent molecules to be calculated, and thus it was possible to produce solvent-free diffraction intensities [28].

2.3. Cyclic voltammetry

Cyclic voltammograms were recorded using an EG&G PAR Model 283 potentiostat operated with M770 v.4.23 software. Airtight, single-compartment, three-electrode cells were used with a 0.422 mm^2 platinum microdisc working electrode polished with 0.25 μm diamond paste, a platinum wire auxiliary electrode and an Ag wire pseudoreference electrode. The ferrocene/ferrocenium (Fc/Fc^+) redox couple served as an internal reference for determination of electrode potentials. The studied samples contained a 10^{-3} M Mo complex and 10^{-1} M Bu_4NPF_6 supporting electrolyte. For some measurements, the voltammetric cell was cooled to 200 K by using an acetone/dry ice slurry.

2.4. Spectroelectrochemistry

IR spectroelectrochemical experiments were performed using a Bruker Vertex 70v FT-IR spectrometer either equipped with a DTGS detector or connected to a separate Bio-Rad FTS 60 MCT detector unit (for measurements at 183 K). UV–Vis spectroelectrochemistry was performed using a Scinco S-3100 diode-array spectrophotometer.

Thin-layer UV–Vis and IR spectroelectrochemical measurements were carried out at 293 K (THF, PrCN) and 183 K (PrCN) using OTTLE cells [29–31] equipped with Pt minigrid working and auxiliary electrodes, an Ag microwire pseudoreference electrode and CaF_2 windows. The course of spectroelectrochemical experiments was monitored by thin-layer cyclic voltammetry conducted with a PA4 potentiostat (Laboratory Devices, Polná, Czech Republic). The studied samples contained a 10^{-3} M (UV–Vis spectroelectrochemistry) or 3 × 10^{-3} M (IR spectroelectrochemistry) Mo complex and 3 × 10^{-1} M Bu_4NPF_6 supporting electrolyte.

3. Results and discussion

3.1. Crystal structure of [Mo(CO)$_2$(η^3-allyl)(2,6-xylyl-BIAN)(NCS)]

The crystal structure for the green complex [$Mo^{II}(CO)_2(\eta^3$-allyl)(2,6-xylyl-BIAN)(NCS)] shows that it has the asymmetric B-type structure with the allyl ligand trans to one of the imino-N coordination sites (Fig. 1). This is in contrast to the structure of the red [$Mo^{II}(CO)_2(\eta^3$-allyl)(bpy)(NCS)] complex [24], which is A-type. The bond lengths in the 2,6-xylyl-BIAN complex are similar to those reported for [$Mo^{II}(CO)_2(\eta^3$-allyl)(bpy)(NCS)], although the α-diimine and NCS Mo–N and carbonyl M–C bonds are slightly longer and the CO and CS bonds slightly shorter for the [Mo^{II}($CO)_2(\eta^3$-allyl)(2,6-xylyl-BIAN)(NCS)] complex with the stronger π-accepting 2,6-xylyl-BIAN ligand compared to 2,2′-bipyridine.

It is remarkable that regardless of the much stronger π-acceptor nature of the 2,6-xylyl-BIAN ligand compared to that of 2,2′-bipyridine (bpy), which is confirmed for the studied complexes [Mo(CO)$_2(\eta^3$-allyl)(L∩L)(NCS)] by the large difference in their redox potentials (Table 2), the ν(CO) wavenumbers of these complexes are very similar (see Experimental and Table 3). A plausible explanation for this surprising observation is the position of the strong donor NCS^- ligand trans to one of the carbonyls in the structure B, whereas both carbonyls bind trans to the nitrogen atoms of the acceptor bpy ligand in the structure A (Chart 1).

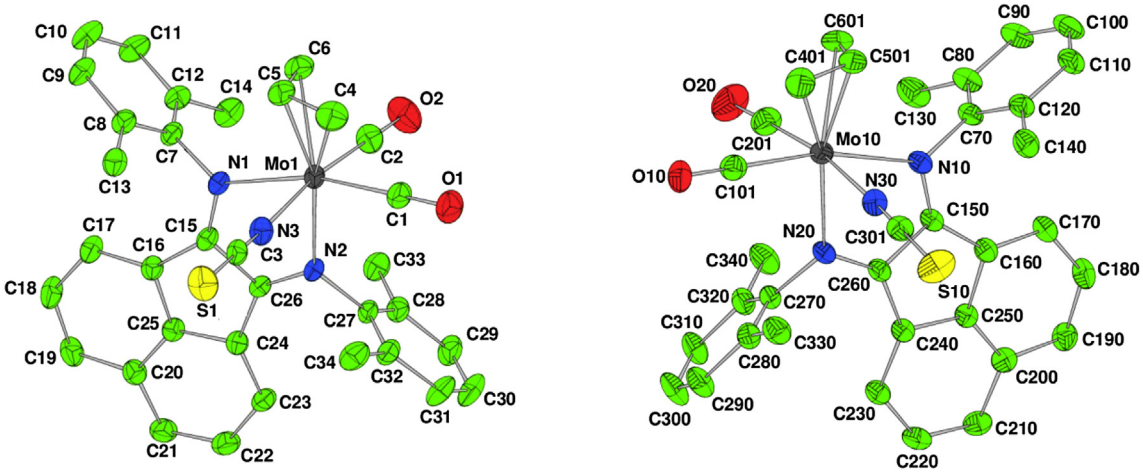

Fig. 1. The two molecules of [$Mo^{II}(CO)_2(\eta^3$-allyl)(2,6-xylyl-BIAN)(NCS)] found in the asymmetric unit. Thermal ellipsoids are shown at 50% probability. Hydrogen atoms are omitted for clarity. Selected bond lengths (Å): Mo(1)–N(1) 2.2863(17); Mo(10)–N(10) 2.2948(16); Mo(1)–N(2) 2.2298(16); Mo(10)–N(20) 2.2314(16); Mo(1)–N(3) 2.1828(18); Mo(10)–N(30) 2.1819(19); Mo(1)–C(1) 1.975(2); Mo(10)–C(101) 1.954(2); Mo(1)–C(2) 1.959(2); Mo(10)–C(201) 1.968(3); Mo(1)–C(4) 2.325(2); Mo(10)–C(401) 2.336(2); Mo(1)–C(5) 2.191(2); Mo(10)–C(501) 2.208(2); Mo(1)–C(6) 2.309(2); Mo(10)–C(601) 2.325(2); N(3)–C(3) 1.169(3); N(30)–C(301) 1.162(3); S(1)–C(3) 1.622(2); S(10)–C(301) 1.627(2); O(1)–C(1) 1.156(3); O(10)–C(101) 1.159(3); O(2)–C(2) 1.152(3); O(20)–C(201) 1.157(3). Selected bond angles (°): N(1)–Mo(1)–N(2) 73.41(6); N(10)–Mo(10)–N(20) 73.33(6); C(1)–Mo(1)–C(2) 79.48(10); C(101)–Mo(10)–C(201) 77.14(10).

Table 2
Electrochemical potentials for $[Mo(CO)_2(\eta^3\text{-allyl})(L\cap L)(NCS)]$ (L∩L = bpy, 2,6-xylyl-BIAN) and their reduction products.

Complex	Solvent	$E_{p,a}$/V		$E_{p,c}$/V	
$[Mo(CO_2)(\eta^3\text{-allyl})(bpy)(NCS)]$	THF	$Mo^{II/III}$	0.20[a]	R1	−1.99
	PrCN	$Mo^{II/III}$	0.22[a]	R1	−1.95
				R1/O1	−1.89[a,c]
$[Mo(CO_2)(\eta^3\text{-allyl})(2,6\text{-xylyl-BIAN})(NCS)]$	THF	$Mo^{II/III}$	0.59	R1/O1	−1.16[a]
$[Mo(CO_2)(\eta^3\text{-allyl})(bpy^{\bullet-})(NCS)]^-$	PrCN	O1	−1.88[b]	R2	−2.54[b]
				R2	−2.58[c]
$[Mo(CO_2)(\eta^3\text{-allyl})(2,6\text{-xylyl-BIAN}^{\bullet-})(NCS)]^-$	THF			R2	−2.09
$[Mo(CO_2)(\eta^3\text{-allyl})(bpy)]_2$	THF			R(D)	−2.52
	PrCN	O(D)	−0.63[c]		
$[Mo(CO_2)(\eta^3\text{-allyl})(bpy)]^-$	THF	O1′	−1.74	R2′	−2.82
	PrCN	O1′	−1.74	R2′	−2.77
$[Mo(CO_2)(\eta^3\text{-allyl})(2,6\text{-xylyl-BIAN})(THF)]^-$	THF			R2′	−3.11

[a] $E_{1/2}$ value.
[b] Recorded at 2 V s^{-1}.
[c] Recorded at 200 K.

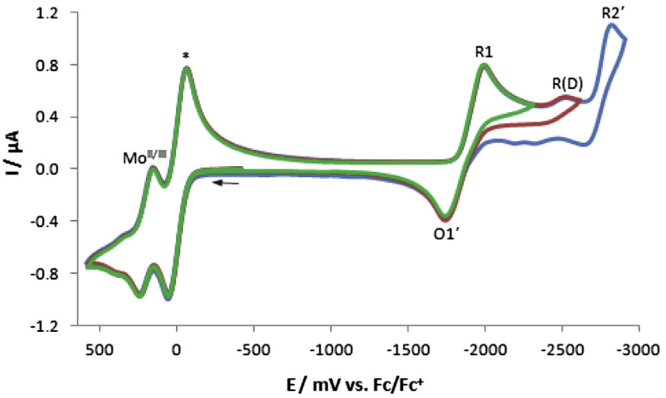

Fig. 2. Cyclic voltammogram of $[Mo(CO)_2(\eta^3\text{-allyl})(bpy)(NCS)]$ in the THF/Bu_4NPF_6 electrolyte at room temperature recorded at a scan rate of 100 mV s^{-1}. The Fc/Fc^+ standard redox couple is marked with an asterisk.

The formation of the B-type structure for $[Mo^{II}(CO)_2(\eta^3\text{-allyl})(2,6\text{-xylyl-BIAN})(NCS)]$ is likely to arise from a combination of steric and electronic factors, such as the bulkiness of the substituted 2,6-xylyl-BIAN ligand giving rise to possible interaction of the 2,6-xylyl substituent with the allyl ligand [32], and the strongly π-accepting nature of the 2,6-xylyl-BIAN ligand. Indeed, it has been previously reported [12,13] that complexes with strongly π-accepting diphosphine and diarsine ligands, rather than donor α-diimine ligands, are more likely to form the asymmetric B-type structure. The latter has also been reported for the related tricarbonyl cationic complexes $[Mo(CO)_3(\eta^3\text{-}C_3H_4Me)(Ar\text{-BIAN})]^+$ (Ar = 2-Me-C_6H_4, 2,6-^{i}Pr$_2$-C_6H_3) [33].

3.2. Cyclic voltammetry of $[Mo(CO)_2(\eta^3\text{-allyl})(bpy)(NCS)]$

3.2.1. In THF at room temperature

The electrochemical behaviour of $[Mo(CO)_2(\eta^3\text{-allyl})(bpy)(NCS)]$ was initially studied using cyclic voltammetry (Fig. 2). In THF, this complex undergoes reversible Mo(II) → Mo(III) oxidation at $E_{1/2}$ = 0.20 V vs. Fc/Fc^+, as reported in the literature [17,18].

The irreversible cathodic wave, R1, of $[Mo(CO)_2(\eta^3\text{-allyl})(bpy)(NCS)]$ is observed at $E_{p,c}$ = −1.99 V (THF at ambient temperature) with an anodic peak, O1′, seen on the reverse scan at $E_{p,a}$ = −1.75 V. At higher scan rates in THF (Fig. 3), or in PrCN at lower temperatures recorded (see below), this is accompanied by a second anodic peak, O1, due to the increased stability of the $[Mo(CO)_2(\eta^3\text{-allyl})(bpy^{\bullet-})(NCS)]^-$ radical anion. From the combination of cyclic voltammetry and spectroelectrochemical results (discussed below), and comparison with the well known $[Mn(CO)_3(bpy)Cl]$ system [19,20], the anodic peak O1′ has been assigned to oxidation of the five-coordinate anion, $[Mo(CO)_2(\eta^3\text{-allyl})(bpy)]^-$.

The reduction of $[Mo(CO)_2(\eta^3\text{-allyl})(bpy)(NCS)]$ to unstable $[Mo(CO)_2(\eta^3\text{-allyl})(bpy^{\bullet-})(NCS)]^-$ (Equation (1)) results in concomitant dissociation of NCS^- to give the five-coordinate radical $[Mo(CO)_2(\eta^3\text{-allyl})(bpy^{\bullet-})]$ (Equation (2)). $[Mo(CO)_2(\eta^3\text{-allyl})(bpy^{\bullet-})]$ undergoes $1e^-$ reduction to $[Mo(CO)_2(\eta^3\text{-allyl})(bpy)]^-$ (Equation (3)) directly at the potential of the parent complex, as indicated by the O1′ anodic counterwave. This behaviour is very similar to that observed for the related $[Mn(CO)_3(bpy)Cl]$ complex, where the unstable $[Mn(CO)_3(bpy^{\bullet-})Cl]^-$ radical anion formed upon the $1e^-$ reduction instantaneously loses the Cl^- ligand and the resulting five-coordinate radical undergoes directly a second $1e^-$ reduction (ECE) to give $[Mn(CO)_3(bpy)]^-$ [19,20].

$[Mo(CO)_2(\eta^3\text{-allyl})(bpy)]^-$ is able to react with the yet non-reduced parent complex to form a dimer, $[Mo(CO)_2(\eta^3\text{-allyl})(bpy)]_2$ (Equation (4)), as is also observed in the case of $[Mn(CO)_3(bpy)]^-$ [19,20]. The cathodic wave R(D) at $E_{p,c}$ = −2.52 V corresponds to the reduction of $[Mo(CO)_2(\eta^3\text{-allyl})(bpy)]_2$ to $[Mo(CO)_2(\eta^3\text{-allyl})(bpy)]_2^{\bullet-}$ (Equation (5)), which dissociates to give a combination of $[Mo(CO)_2(\eta^3\text{-allyl})(bpy)]^-$ and $[Mo(CO)_2(\eta^3\text{-allyl})(bpy^{\bullet-})]$ (Equation (6)). The latter transient radical undergoes immediate reduction to give a second molecule of $[Mo(CO)_2(\eta^3\text{-allyl})(bpy)]^-$. Reduction of $[Mo(CO)_2(\eta^3\text{-allyl})(bpy)]^-$ occurs on the R2′ cathodic peak at $E_{p,c}$ = −2.82 V.

Table 3
IR and UV–Vis absorption data for $[Mo(CO)_2(\eta^3\text{-allyl})(L\cap L)(NCS)]$ (L∩L = bpy, 2,6-xylyl-BIAN) and their reduction products.

Complex	Solvent[a]	ν(CO)/cm^{-1}	ν(NC)/cm^{-1}	λ_{max}/nm
$[Mo(CO_2)(\eta^3\text{-allyl})(2,6\text{-xylyl-BIAN})(NCS)]$	THF	1946, 1872	2075	331, 373, 715
$[Mo(CO_2)(\eta^3\text{-allyl})(2,6\text{-xylyl-BIAN}^{\bullet-})(NCS)]^-$	THF	1918, 1830	2090	408, 508
$[Mo(CO_2)(\eta^3\text{-allyl})(2,6\text{-xylyl-BIAN})(THF)]^-$	THF	1885, 1798		
$[Mo(CO_2)(\eta^3\text{-allyl})(bpy)(NCS)]$	THF	1951, 1871	2075	340, 501
	MeCN	1950, 1866	2083	
	PrCN	1950, 1868	2079	351, 478
	PrCN[b]	1946, 1864	2085	
$[Mo(CO_2)(\eta^3\text{-allyl})(bpy^{\bullet-})(NCS)]^-$	PrCN[b]	1920, 1829	2092	
$[Mo(CO_2)(\eta^3\text{-allyl})(bpy)(PrCN)]^-$	PrCN[b]	1893, 1796	2147	
$[Mo(CO_2)(\eta^3\text{-allyl})(bpy)]_2$	THF	1891, 1778, 1757		369, 581
	PrCN	1892, 1775		371, 538
$[Mo(CO_2)(\eta^3\text{-allyl})(bpy)]^-$	THF	1844, 1723		388, 551, 585, 632, 735, 829

[a] The solvent contained the supporting electrolyte, 3×10^{-1} M Bu_4NPF_6.
[b] Recorded in PrCN at 183 K. All other spectra recorded at room temperature.

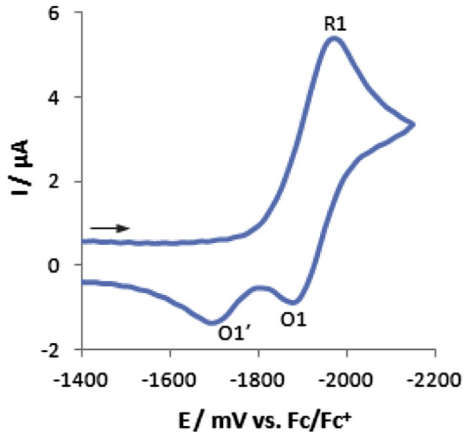

Fig. 3. Cyclic voltammogram of $[Mo(CO)_2(\eta^3\text{-allyl})(bpy)(NCS)]$ in the THF/Bu_4NPF_6 electrolyte at room temperature recorded at a scan rate of 2 V s^{-1}.

$$\left[Mo(CO)_2(\eta^3-\text{allyl})(bpy)(NCS)\right] + e^- \leftrightarrow \left[Mo(CO)_2(\eta^3-\text{allyl})(bpy^{\bullet-})(NCS)\right]^- \quad R1 \tag{1}$$

$$\left[Mo(CO)_2(\eta^3-\text{allyl})(bpy^{\bullet-})(NCS)\right]^- \rightarrow \left[Mo(CO)_2(\eta^3-\text{allyl})(bpy^{\bullet-})\right] + NCS^- \tag{2}$$

$$\left[Mo(CO)_2(\eta^3-\text{allyl})(bpy^{\bullet-})\right] + e^- \leftrightarrow \left[Mo(CO)_2(\eta^3-\text{allyl})(bpy)\right]^- \quad R1' \tag{3}$$

$$\left[Mo(CO)_2(\eta^3-\text{allyl})(bpy)\right]^- + \left[Mo(CO)_2(\eta^3-\text{allyl})(bpy)(NCS)\right] \rightarrow \left[Mo(CO)_2(\eta^3-\text{allyl})(bpy)\right]_2 + NCS^- \tag{4}$$

$$\left[Mo(CO)_2(\eta^3-\text{allyl})(bpy)\right]_2 + e^- \rightarrow \left[Mo(CO)_2(\eta^3-\text{allyl})(bpy)\right]_2^- \quad R(D) \tag{5}$$

$$\left[Mo(CO)_2(\eta^3-\text{allyl})(bpy)\right]_2^- \rightarrow \left[Mo(CO)_2(\eta^3-\text{allyl})(bpy^{\bullet-})\right] + \left[Mo(CO)_2(\eta^3-\text{allyl})(bpy)\right]^- \tag{6}$$

3.2.2. *In PrCN at room and low temperature*

The cyclic voltammogram of $[Mo(CO)_2(\eta^3\text{-allyl})(bpy)(NCS)]$ was recorded in PrCN to observe the difference in electrochemical behaviour in a more strongly coordinating solvent. In PrCN at room temperature (Fig. S1), the reversible Mo(II) → Mo(III) oxidation is observed at $E_{1/2} = 0.22$ V.

The irreversible bpy-based reduction closely resembles that observed in THF, with the reduction (R1) of $[Mo(CO)_2(\eta^3\text{-allyl})(bpy)(NCS)]$ to $[Mo(CO)_2(\eta^3\text{-allyl})(bpy^{\bullet-})(NCS)]^-$ at $E_{p,c} = -1.95$ V, and the resulting oxidation (O1′) of $[Mo(CO)_2(\eta^3\text{-allyl})(bpy)]^-$ at $E_{p,a} = -1.74$ V. At 200 K (Fig. 4b) or increased scan rates (Fig. 4a), a new cathodic peak (R2) is seen at $E_{p,c} = -2.54$ V, corresponding to the reduction of $[Mo(CO)_2(\eta^3\text{-allyl})(bpy^{\bullet-})(NCS)]^-$ to $[Mo(CO)_2(\eta^3\text{-allyl})(bpy)(NCS)]^{2-}$ (Equation (7)). The unstable dianion immediately dissociates NCS^- and converts to $[Mo(CO)_2(\eta^3\text{-allyl})(bpy)]^-$ (Equation (8)) observed on the reverse anodic scan (O1′).

Unlike in THF, the cathodic peak associated with reduction of the $[Mo(CO)_2(\eta^3\text{-allyl})(bpy)]_2$ dimer in PrCN is barely observable at room temperature on the CV timescale, as the strongly coordinating PrCN solvent may partly inhibit its formation (Equation (9)). An anodic peak, O(D), corresponding to the oxidation of $[Mo(CO)_2(\eta^3\text{-allyl})(bpy)]_2$ is seen more clearly on the reverse anodic scan at 200 K; although, this only appears when first passing the wave R2 where $[Mo(CO)_2(\eta^3\text{-allyl})(bpy)]^-$ is formed, converting to the dimer at O1′ (Fig. 4b).

The reduction of the five-coordinate anion, $[Mo(CO)_2(\eta^3\text{-allyl})(bpy)]^-$, is observed at room temperature at $E_{p,a} = -2.77$ V (cathodic wave R2′). At 200 K (Fig. 4b), this peak is poorly defined, probably due to coordination of PrCN to $[Mo(CO)_2(\eta^3\text{-allyl})(bpy)]^-$ (Equation (9)) revealed by IR spectroelectrochemistry (see below).

$$\left[Mo(CO)_2(\eta^3-\text{allyl})(bpy^{\bullet-})(NCS)\right]^- + e^- \leftrightarrow \left[Mo(CO)_2(\eta^3-\text{allyl})(bpy)(NCS)\right]^{2-} \quad R2 \tag{7}$$

$$\left[Mo(CO)_2(\eta^3-\text{allyl})(bpy)(NCS)\right]^{2-} \rightarrow \left[Mo(CO)_2(\eta^3-\text{allyl})(bpy)\right]^- + NCS^- \tag{8}$$

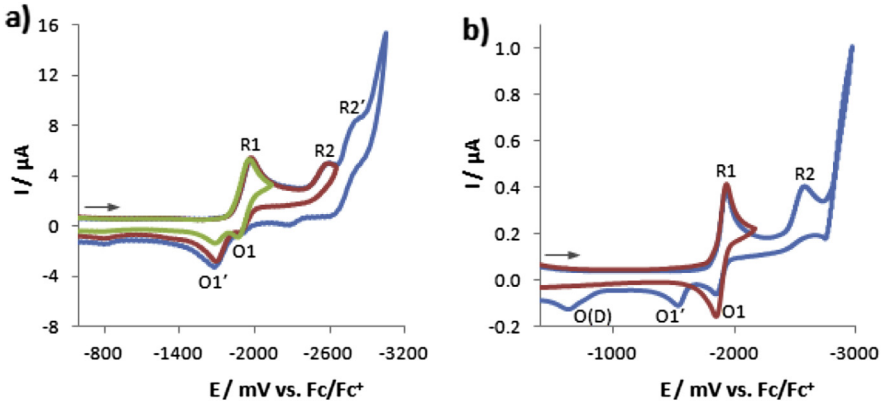

Fig. 4. Cyclic voltammograms of $[Mo(CO)_2(\eta^3\text{-allyl})(bpy)(NCS)]$ in the PrCN/Bu_4NPF_6 electrolyte a) at room temperature, recorded at $v = 2$ V s^{-1}, and b) at 200 K, recorded at $v = 100$ mV s^{-1}.

$$\left[Mo(CO)_2(\eta^3-allyl)(bpy)\right]^- + PrCN \rightarrow \left[Mo(CO)_2(\eta^3-allyl)(bpy)(PrCN)\right]^- \quad (9)$$

3.3. Cyclic voltammetry of [Mo(CO)$_2$(η^3-allyl)(2,6-xylyl-BIAN)(NCS)]

The electrochemical behaviour of the [Mo(CO)$_2$(η^3-allyl)(2,6-xylyl-BIAN)(NCS)] complex was studied in THF (Fig. 5). The anodic scan shows that, unlike for the analogous bpy complex (see above), the Mo(II)/Mo(III) oxidation at $E_{p,a} = 0.59$ V is irreversible. The 2,6-xylyl-BIAN ligand is a much stronger π-acceptor than bpy which enables it to stabilize the radical anion produced on the initial reduction of [Mo(CO)$_2$(η^3-allyl)(2,6-xylyl-BIAN)(NCS)], but less able than bpy to stabilize the formally Mo(III) species produced upon the oxidation.

On the cathodic scan, the initial 2,6-xylyl-BIAN-based redox couple (R1/O1) is observed at $E_{1/2} = -1.16$ V. This process is both chemically and electrochemically reversible (Fig. 6), and is significantly positively shifted compared with the analogous reduction of the bpy complex as a result of the extended π-aromatic system of the 2,6-xylyl-BIAN ligand and a low-lying LUMO, which stabilizes the 1e$^-$ reduced species, [Mo(CO)$_2$(η^3-allyl)(2,6-xylyl-BIAN$^{\bullet-}$)(NCS)]$^-$ (Equation (10)). The second cathodic wave R2 lies at $E_{p,c} = -2.09$ V and is irreversible due to dissociation of the NCS$^-$ ligand from the [Mo(CO)$_2$(η^3-allyl)(2,6-xylyl-BIAN)(NCS)]$^{2-}$ dianion to produce [Mo(CO)$_2$(η^3-allyl)(2,6-xylyl-BIAN)]$^-$ (Equations (11) and (12)), as revealed by IR spectroelectrochemistry (see below).

A further cathodic peak, R2′, is seen at $E_{p,c} = -3.11$ V. The negative potential shift of R2′ from the R1 and R2 waves for the 2,6-xylyl-BIAN complex is larger than was the case for the bpy complex. This difference suggests that, unlike in the related bpy complex, the five coordinate anion [Mo(CO)$_2$(η^3-allyl)(2,6-xylyl-BIAN)]$^-$ with the strong π-acceptor α-diimine ligand is capable of coordinating the donor solvent (even THF) on the CV timescale (Equation (13)). The cathodic spectroelectrochemical data in THF support this assumption (see below).

$$\left[Mo(CO)_2(\eta^3-allyl)(2,6-xylyl-BIAN)(NCS)\right] + e^- \leftrightarrow \left[Mo(CO)_2(\eta^3-allyl)(2,6-xylyl-BIAN^{\bullet-})(NCS)\right]^- \quad R1 \quad (10)$$

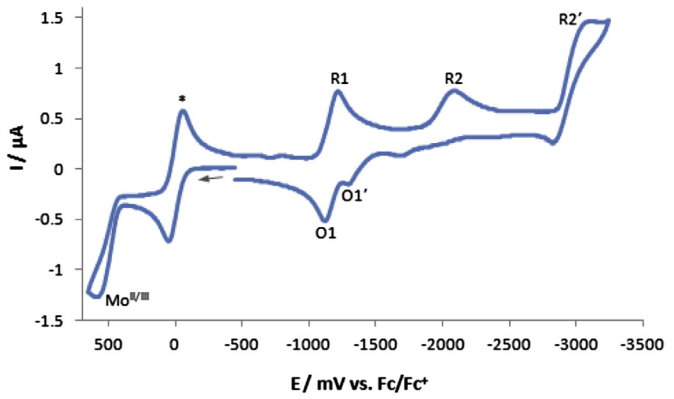

Fig. 5. Cyclic voltammogram of [Mo(CO)$_2$(η^3-allyl)(2,6-xylyl-BIAN)(NCS)] in the THF/Bu_4NPF_6 electrolyte at room temperature recorded at a scan rate of 100 mV s^{-1}. The Fc/Fc$^+$ standard redox couple is marked with an asterisk.

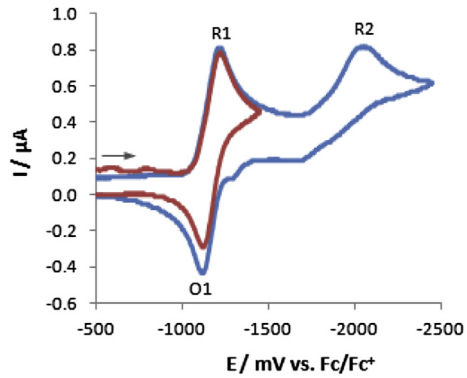

Fig. 6. Cyclic voltammogram of [Mo(CO)$_2$(η^3-allyl)(2,6-xylyl-BIAN)(NCS)] in the THF/Bu_4NPF_6 electrolyte at room temperature recorded at a scan rate of 100 mV s^{-1}.

$$\left[Mo(CO)_2(\eta^3-allyl)(2,6-xylyl-BIAN^{\bullet-})(NCS)\right]^- + e^- \leftrightarrow \left[Mo(CO)_2(\eta^3-allyl)(2,6-xylyl-BIAN)(NCS)\right]^{2-} \quad R2 \quad (11)$$

$$\left[Mo(CO)_2(\eta^3-allyl)(2,6-xylyl-BIAN)(NCS)\right]^{2-} \rightarrow \left[Mo(CO)_2(\eta^3-allyl)(2,6-xylyl-BIAN)\right]^- + NCS^- \quad (12)$$

$$\left[Mo(CO)_2(\eta^3-allyl)(2,6-xylyl-BIAN)\right]^- + THF \rightarrow \left[Mo(CO)_2(\eta^3-allyl)(2,6-xylyl-BIAN)(THF)\right]^- \quad (13)$$

3.4. Spectroelectrochemistry of [Mo(CO)$_2$(η^3-allyl)(bpy)(NCS)]: oxidation

The oxidation of [Mo(CO)$_2$(η^3-allyl)(bpy)(NCS)] was shown to be reversible at room temperature using cyclic voltammetry at $v \geq 100$ mV s^{-1} (Fig. 6). An IR monitored rapid potential step oxidation was carried out in MeCN at room temperature (Fig. 7) to identify and characterise the [Mo^{III}(CO)$_2$(η^3-allyl)(bpy)(NCS)]$^+$ cations.

On the timescale of seconds, the ν(CO) bands at 1950 and 1866 cm^{-1} and the ν(CN) band at 2083 cm^{-1} are replaced by a narrow ν(CO) band at 2069 cm^{-1} and a broader, more intense band at 2028 cm^{-1} resulting from overlap of the ν(CN) and second ν(CO) bands. [Mo^{III}(CO)$_2$(η^3-allyl)(bpy)(NCS)]$^+$ is not completely stable under these conditions, with the decrease of the ν(CO) band at 2069 cm^{-1} accompanied by the increase of the ν(CN) band at 2028 cm^{-1} indicating decarbonylation. Low intensity ν(CO) bands are observed at 1959 and 1875 cm^{-1}, with the small shift in wavenumbers pointing to the presence of a secondary (less electron rich) Mo(II) species.

Anodic IR spectroelectrochemistry was carried out on [Mo(CO)$_2$(η^3-allyl)(bpy)(NCS)] in PrCN at 183 K (Fig. 8) where [Mo^{III}(CO)$_2$(η^3-allyl)(bpy)(NCS)]$^+$ becomes completely stable. The ν(CO) bands of [Mo(CO)$_2$(η^3-allyl)(bpy)(NCS)] at 1947 and 1864 cm^{-1} shift to 2069 and 2019 cm^{-1} upon oxidation to [Mo(CO)$_2$(η^3-allyl)(bpy)(NCS)]$^+$, accompanied by the shift of the ν(CN) band of the thiocyanate ligand from 2085 to 2034 cm^{-1}. The shift of the ν(CO) bands is in good agreement with the values reported in the literature for the related species [Mo^{III}(CO)$_2$(η^3-allyl)(bpy)Cl]$^+$ and [Mo^{III}(CO)$_2$(η^3-allyl)(bpy)(O_2CCF_3)]$^+$ [18]. The

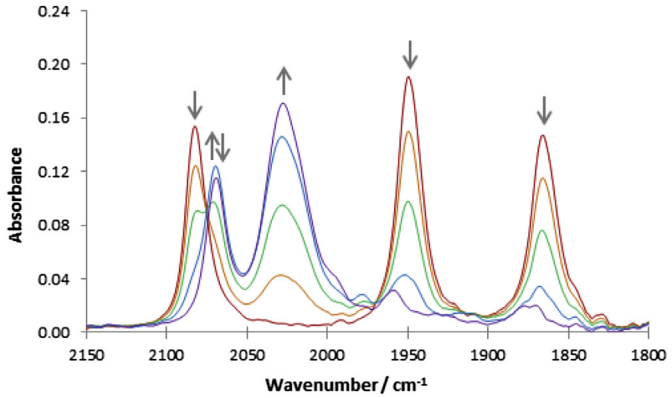

Fig. 7. Infrared spectroelectrochemistry of $[Mo(CO)_2(\eta^3\text{-allyl})(bpy)(NCS)]$ (↓) in the $MeCN/Bu_4NPF_6$ electrolyte, showing the potential-step oxidation to $[Mo(CO)_2(\eta^3\text{-allyl})(bpy)(NCS)]^+$ within an OTTLE cell at room temperature. The ν(CO) band labelled with ↑↓ indicates the slow decomposition of the primary cationic product (see the main text).

ν(CN) band of the thiocyanate ligand shifts to lower wavenumbers upon oxidation as the π-donation from the anionic ligand to the metal increases, and the Mo═N═C═S resonance form of the ligand becomes more favourable.

3.5. Spectroelectrochemistry of $[Mo(CO)_2(\eta^3\text{-allyl})(2,6\text{-xylyl-BIAN})(NCS)]$: oxidation

Cyclic voltammetry has shown that the predominantly metal-based $1e^-$ oxidation of $[Mo(CO)_2(\eta^3\text{-allyl})(2,6\text{-xylyl-BIAN})(NCS)]$ is irreversible at moderate scan rates (Fig. 5). IR spectroelectrochemistry was used to monitor the ν(CO) and ν(CN) absorption bands during this process (Fig. S2).

Upon oxidation in THF at ambient temperature, the parent ν(CO) bands at 1946 and 1872 cm^{-1} were lost, accompanied by the appearance of low intensity ν(CO) bands at 1960 and 1887 cm^{-1} due to a secondary Mo(II) species. The ν(CN) band of the thiocyanate ligand shifted from 2075 to 2022 cm^{-1}, a value similar to the wavenumbers of the decarbonylated product observed for decomposition of $[Mo(CO)_2(\eta^3\text{-allyl})(bpy)(NCS)]^+$ in THF. No band was seen at 2055 cm^{-1} corresponding to free NCS^- [34], indicating that this ligand remains coordinated to the unknown ultimate oxidation product.

3.6. Spectroelectrochemistry of $[Mo(CO)_2(\eta^3\text{-allyl})(2,6\text{-xylyl-BIAN})(NCS)]$: reduction

It was shown with cyclic voltammetry that the initial reduction of $[Mo(CO)_2(\eta^3\text{-allyl})(bpy)(NCS)]$ was irreversible (Fig. 2), whereas a reversible reduction was seen for the analogous $[Mo(CO)_2(\eta^3\text{-allyl})(2,6\text{-xylyl-BIAN})(NCS)]$ complex (Fig. 6). IR spectroelectrochemistry was used to study the initial reversible reduction of $[Mo(CO)_2(\eta^3\text{-allyl})(2,6\text{-xylyl-BIAN})(NCS)]$ in THF and to identify the product formed (Fig. 9).

IR monitoring of the initial cathodic step of $[Mo(CO)_2(\eta^3\text{-allyl})(2,6\text{-xylyl-BIAN})(NCS)]$ at $E_{1/2} = -1.16$ V shows the shift of the ν(CO) bands from 1946 and 1872 cm^{-1} to 1918 and 1830 cm^{-1} belonging to stable $[Mo(CO)_2(\eta^3\text{-allyl})(2,6\text{-xylyl-BIAN}^{\bullet-})(NCS)]^-$. The ν(CN) band shifts from 2075 to 2090 cm^{-1} as the thiocyanate ligand tends towards the less π-donating Mo—N≡C—S^- resonance form. The UV—Vis spectroelectrochemistry (Fig. 10) of this largely 2,6-xylyl-BIAN-localised $1e^-$ reduction shows the intense absorption band of the parent complex at 715 nm replaced by a band at 522 nm due to $[Mo(CO)_2(\eta^3\text{-allyl})(2,6\text{-xylyl-BIAN}^{\bullet-})(NCS)]^-$, in a good agreement with the UV—Vis spectrum of the free 2,6-xylyl-$BIAN^{\bullet-}$ radical anion (Fig. 10 inset).

The subsequent irreversible reduction of $[Mo(CO)_2(\eta^3\text{-allyl})(2,6\text{-xylyl-BIAN}^{\bullet-})(NCS)]^-$ at −2.09 V (R2) results in rapid dissociation of the NCS^- ligand, as evidenced by the new ν(CN) band at 2056 cm^{-1} [34] (Fig. 11). The two new ν(CO) bands arising at 1885 and 1798 cm^{-1} most likely belong to the $2e^-$-reduced anion $[Mo(CO)_2(\eta^3\text{-allyl})(2,6\text{-xylyl-BIAN})(THF)]^-$ (Equations (11)–(13)), as deduced from the cyclic voltammetric data (see above). Another support for this assignment comes from similar CO-stretching wavenumbers of the closely related six-coordinate anion, $[Mo(CO)_2(\eta^3\text{-allyl})(bpy)(PrCN)]^-$, that was found stable only at 183 K (see Table 3). In contrast, $[Mo(CO)_2(\eta^3\text{-allyl})(2,6\text{-xylyl-BIAN})(THF)]^-$ is stable already at room temperature, despite the weaker coordination of THF compared to PrCN, which can be ascribed to the dominant localization of the second cathodic step at the 2,6-xylyl-BIAN ligand. In this respect, doubly reduced bpy is a much stronger π-donor, stabilizing the 5-coordinate geometry of $[Mo(CO)_2(\eta^3\text{-allyl})(bpy)]^-$ in THF (see below) and only PrCN can bind at low temperature. These observations comply with the reduction paths previously reported for $[Re(CO)_3(\alpha\text{-diimine})X]$ (X = halide) involving both five-coordinate anions $[Re(CO)_3(\alpha\text{-diimine})]^-$ (for donor α-diimine ligands) and their six-coordinate equivalents $[Re(CO)_3(\alpha\text{-diimine})X]^{n-}$ ($n = 1$, X = donor solvent; $n = 2$, X = halide) [35].

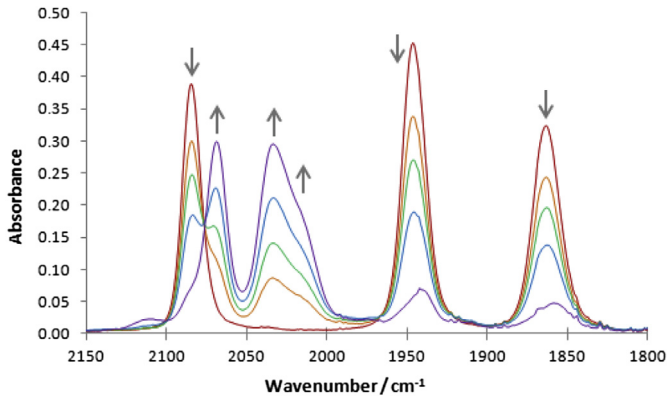

Fig. 8. Infrared spectroelectrochemistry of $[Mo(CO)_2(\eta^3\text{-allyl})(bpy)(NCS)]$ (↓) in the $PrCN/Bu_4NPF_6$ electrolyte, showing oxidation to inert $[Mo(CO)_2(\eta^3\text{-allyl})(bpy)(NCS)]^+$ (↑) within an OTTLE cell at 183 K.

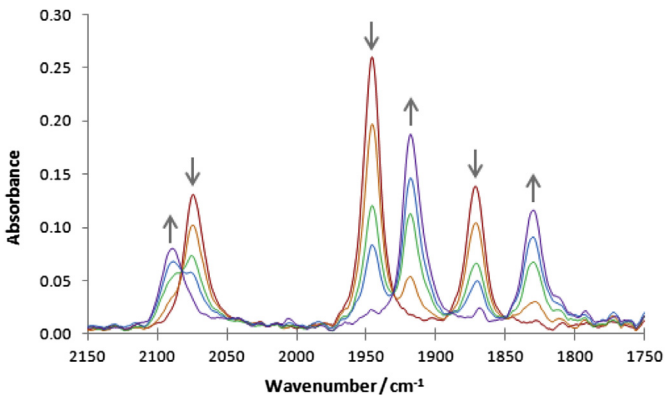

Fig. 9. Infrared spectroelectrochemistry of $[Mo(CO)_2(\eta^3\text{-allyl})(2,6\text{-xylyl-BIAN})(NCS)]$ (↓) in the THF/Bu_4NPF_6 electrolyte, showing reduction to $[Mo(CO)_2(\eta^3\text{-allyl})(2,6\text{-xylyl-BIAN}^{\bullet-})(NCS)]^-$ (↑) within an OTTLE cell at room temperature.

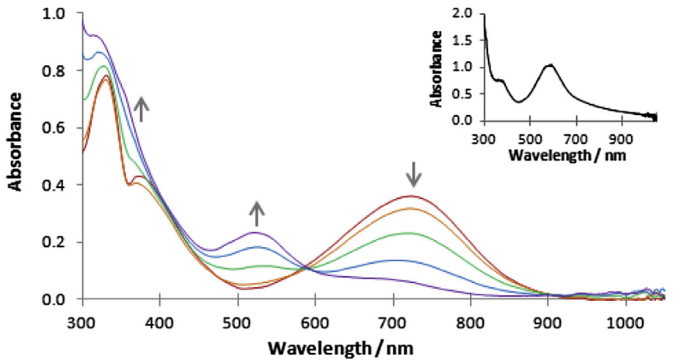

Fig. 10. UV–Vis spectroelectrochemistry of $[Mo(CO)_2(\eta^3\text{-allyl})(2,6\text{-xylyl-BIAN})(NCS)]$ (↓) in the THF/Bu_4NPF_6 electrolyte, showing the reduction to $[Mo(CO)_2(\eta^3\text{-allyl})(2,6\text{-xylyl-BIAN}^{\bullet-})(NCS)]^-$ (↑) within an OTTLE cell at room temperature. Inset: the UV–Vis spectrum of free $[2,6\text{-xylyl-BIAN}]^{\bullet-}$ in THF generated under the same conditions.

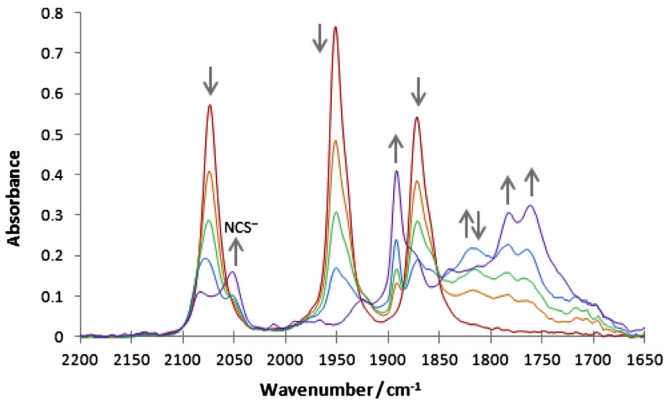

Fig. 12. Infrared spectroelectrochemistry of $[Mo(CO)_2(\eta^3\text{-allyl})(bpy)(NCS)]$ (↓) in the THF/Bu_4NPF_6 electrolyte, showing initial reduction and formation of $[Mo(CO)_2(\eta^3\text{-allyl})(bpy)]_2$ (↑) within an OTTLE cell at room temperature.

3.7. Spectroelectrochemistry of $[Mo(CO)_2(\eta^3\text{-allyl})(bpy)(NCS)]$: reduction

3.7.1. In THF at room temperature

The initial $1e^-$ reduction of $[Mo(CO)_2(\eta^3\text{-allyl})(bpy)(NSC)]$ at −2.05 V is irreversible at room temperature, as seen by cyclic voltammetry (Fig. 2). IR monitoring of this cathodic reaction in THF (Fig. 12) shows a decay of the ν(CN) and ν(CO) bands of the parent complex at 2075 cm^{-1}, and 1951 and 1871 cm^{-1}, respectively. A new ν(CN) band at 2053 cm^{-1} confirms that the NCS^- ligand has dissociated [34].

As discussed above, the loss of the NCS^- ligand from $[Mo(CO)_2(\eta^3\text{-allyl})(bpy^{\bullet-})(NCS)]^-$ results in the formation of a five-coordinate radical, $[Mo(CO)_2(\eta^3\text{-allyl})(bpy^{\bullet-})]$, which is itself readily reduced at −2.05 V to the five-coordinate anion, $[Mo(CO)_2(\eta^3\text{-allyl})(bpy)]^-$ (Equations (1)–(3)). The final product observed is the dimer, $[Mo(CO)_2(\eta^3\text{-allyl})(bpy)]_2$, resulting from reaction of $[Mo(CO)_2(\eta^3\text{-allyl})(bpy)]^-$ with the yet non-reduced parent complex (Equation (4)). The dimer has been identified by its three, typically fairly narrow, ν(CO) bands at 1891, 1778, and 1757 cm^{-1}. The average ν(CO) shift accompanying the reduction of $[Mo(CO)_2(\eta^3\text{-allyl})(bpy)(NSC)]$ to $[Mo(CO)_2(\eta^3\text{-allyl})(bpy)]_2$ is comparable with that observed, e.g., for the cathodic conversion of $[Ru^{II}(CH_3)(CO)_2(^i\text{Pr-DAB})(I)]$ (^{i}Pr-DAB = *N*,*N*′-di-isopropyl-1,4-diazabuta-1,3-diene) (ν(CO) at 2024 and 1958 cm^{-1}) to the similar dimer $[Ru(CH_3)(CO)_2(^i\text{Pr-DAB})]_2$ (ν(CO) at 1981, 1951 and 1922 cm^{-1}) in THF at room temperature [36]. Additional small ν(CO) bands observed around 1811 and 1714 cm^{-1} (↑↓ in Fig. 12) remain unassigned. UV–Vis spectroelectrochemical monitoring of this reduction step (Fig. 13) shows the formation of two bands at 369 and 581 nm. The broad shape of this very intense (solvent dependent, Table 3) MLCT band at 581 nm is similar to that observed at 650 nm for the related metal–metal bonded dimer $[Mn(CO)_3(bpy)]_2$ [19,20].

The reduction of $[Mo(CO)_2(\eta^3\text{-allyl})(bpy)]_2$, as shown in Fig. 14, results in the cleavage of the metal–metal bond (Equations (5) and (6)) and the formation of $[Mo(CO)_2(\eta^3\text{-allyl})(bpy)]^-$ with low-energy ν(CO) bands at 1844 and 1723 cm^{-1}. The large shift of the ν(CO) bands of $[Mo(CO)_2(\eta^3\text{-allyl})(bpy)]^-$ from those of the parent complex $[Mo(CO)_2(\eta^3\text{-allyl})(bpy)(NSC)]$ (110–150 cm^{-1}) is similar to the difference observed between the ν(CO) bands of related $[Mn(CO)_3(bpy)Cl]$ and $[Mn(CO)_3(bpy)]^-$ [19,20]. The UV–Vis spectrum (Fig. 15) shows the appearance of an intense band at 388 nm accompanied by a structured visible absorption band with maxima at 551, 585, 632, 735 and 829 nm. This complex pattern in the visible region is characteristic for a family of $2e^-$-reduced five-coordinate carbonyl anions containing the bpy ligand, such as $[Mn(CO)_3(bpy)]^-$ absorbing at 547 nm with shoulders at 465, 607, 690 and 770 nm; the bands correspond to several close-lying MLCT/LLCT transitions [37].

3.7.2. In PrCN at low temperature

The initial reduction of $[Mo(CO)_2(\eta^3\text{-allyl})(bpy)(NCS)]$ in PrCN was first monitored at 183 K using IR spectroelectrochemistry

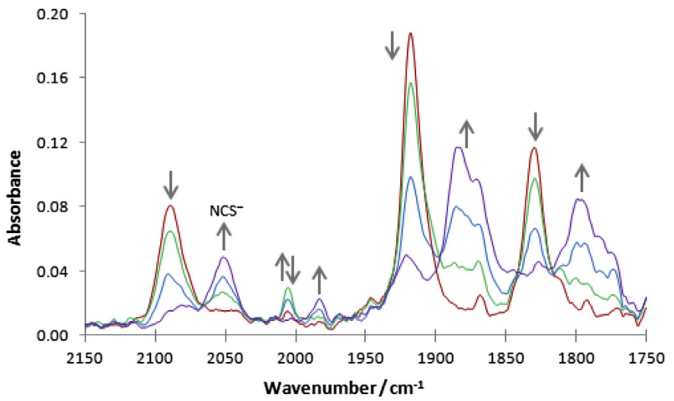

Fig. 11. Infrared spectroelectrochemistry showing the irreversible reduction of $[Mo(CO)_2(\eta^3\text{-allyl})(2,6\text{-xylyl-BIAN}^{\bullet-})(NCS)]^-$ (↓) to $[Mo(CO)_2(\eta^3\text{-allyl})(2,6\text{-xylyl-BIAN})(THF)]^-$ (↑) in the THF/Bu_4NPF_6 electrolyte within an OTTLE cell at room temperature.

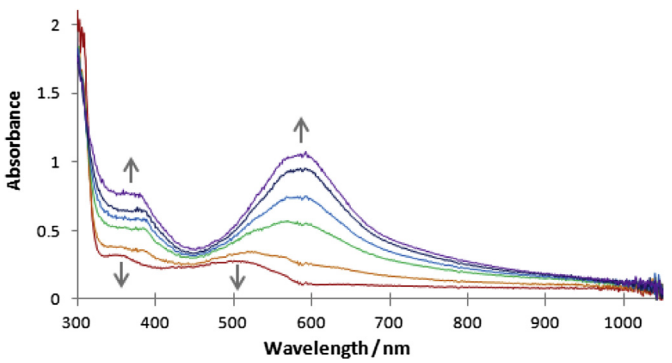

Fig. 13. UV–Vis spectroelectrochemistry of $[Mo(CO)_2(\eta^3\text{-allyl})(bpy)(NCS)]$ (↓) in the THF/Bu_4NPF_6 electrolyte, showing the initial reduction and formation of the dimer $[Mo(CO)_2(\eta^3\text{-allyl})(bpy)]_2$ (↑) within an OTTLE cell at room temperature.

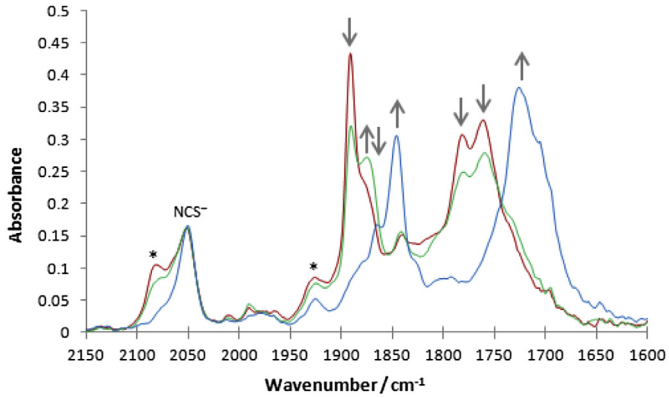

Fig. 14. Infrared spectroelectrochemistry showing the reduction of $[Mo(CO)_2(\eta^3\text{-allyl})(bpy)]_2$ (↓) to $[Mo(CO)_2(\eta^3\text{-allyl})(bpy)]^-$ (↑) in the THF/Bu_4NPF_6 electrolyte, within an OTTLE cell at room temperature. The bands labelled with asterisk belong to remaining $[Mo(CO)_2(\eta^3\text{-allyl})(bpy)(NSC)]$ completely reduced during this step.

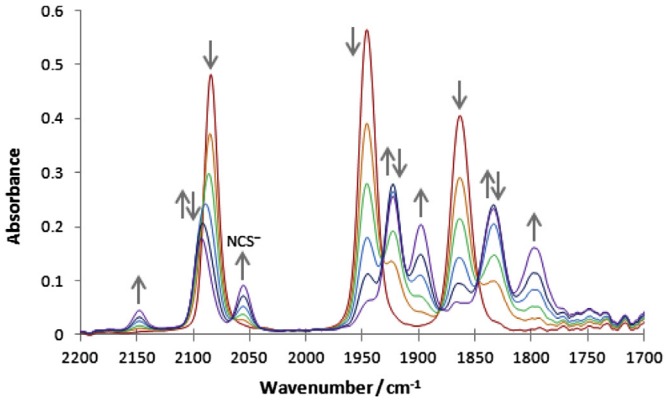

Fig. 16. Infrared spectroelectrochemistry of $[Mo(CO)_2(\eta^3\text{-allyl})(bpy)(NCS)]$ (↓) in the PrCN/Bu_4NPF_6 electrolyte, showing reduction initially to $[Mo(CO)_2(\eta^3\text{-allyl})(bpy^{\bullet-})(NCS)]^-$ (↑↓), then to $[Mo(CO)_2(\eta^3\text{-allyl})(bpy)(PrCN)]^-$ (↑) within an OTTLE cell at 183 K.

(Fig. 16), as cyclic voltammetry has revealed that the reduced temperature results in an increased stability of $[Mo(CO)_2(\eta^3\text{-allyl})(bpy^{\bullet-})(NCS)]^-$. Upon the initial reduction of $[Mo(CO)_2(\eta^3\text{-allyl})(bpy)(NCS)]$ to $[Mo(CO)_2(\eta^3\text{-allyl})(bpy^{\bullet-})(NCS)]^-$, the ν(CO) bands shift from 1946 and 1864 cm^{-1} to 1920 and 1829 cm^{-1}. This is accompanied by the positive shift of the ν(CN) band at 2085 cm^{-1} to 2092 cm^{-1}. The ν(CO) bands shift by 27–35 cm^{-1} and the ν(CN) band by 7 cm^{-1}, i.e., in good agreement with the shifts of 30–47 cm^{-1} and 6 cm^{-1}, respectively, observed for reduction of $[Mo(CO)_2(\eta^3\text{-allyl})(2,6\text{-xylyl-BIAN})(NCS)]$ to $[Mo(CO)_2(\eta^3\text{-allyl})(2,6\text{-xylyl-BIAN}^{\bullet-})(NCS)]^-$ (Fig. 9).

The radical anion $[Mo(CO)_2(\eta^3\text{-allyl})(bpy^{\bullet-})(NCS)]^-$ is not completely stable at 183 K, as shown by the simultaneous growth of the ν(CN) band of free NCS^- at 2056 cm^{-1}, and the appearance of a secondary species with ν(CO) bands at 1893 and 1796 cm^{-1}. The latter reduction product is formed in parallel with $[Mo(CO)_2(\eta^3\text{-allyl})(bpy^{\bullet-})(NCS)]^-$, so it must result from the dissociation of NCS^- and subsequent reduction of the five-coordinate radical $[Mo(CO)_2(\eta^3\text{-allyl})(bpy^{\bullet-})]$ to $[Mo(CO)_2(\eta^3\text{-allyl})(bpy)]^-$, as discussed previously (Equations (1)–(3)). The ν(CO) bands of the stable secondary product lie at much larger wavenumbers than would be expected for $[Mo(CO)_2(\eta^3\text{-allyl})(bpy)]^-$ (1844 and 1723 cm^{-1} in THF at room temperature, Fig. 14). This difference, together with the observation of a band rising at 2147 cm^{-1} and likely belonging to the CN-stretch of a coordinated PrCN molecule [38], point to the formation of the 6-coordinate (solvento) anion $[Mo(CO)_2(\eta^3\text{-allyl})(bpy)(PrCN)]^-$ (Equation (9)). From Table 3, the ν(CO) values for both solvento anions observed $[Mo(CO)_2(\eta^3\text{-allyl})(2,6\text{-xylyl-BIAN})(THF)]^-$ and $[Mo(CO)_2(\eta^3\text{-allyl})(bpy)(PrCN)]^-$ are indeed very similar.

3.7.3. In PrCN at room temperature

Reduction of $[Mo(CO)_2(\eta^3\text{-allyl})(bpy)(NSC)]$ in PrCN at room temperature was monitored with spectroelectrochemistry to investigate differences from the well documented cathodic path in the less coordinating THF electrolyte (see above). Cyclic voltammetry showed that the R(D) cathodic peak corresponding to the reduction of the dimer $[Mo(CO)_2(\eta^3\text{-allyl})(bpy)]_2$ was not perceptible in PrCN (Fig. S1), and evidence for the PrCN coordination and absence of $[Mo(CO)_2(\eta^3\text{-allyl})(bpy)]_2$ was obtained by IR spectroelectrochemistry at 183 K (Fig. 16).

The IR spectrum of $[Mo(CO)_2(\eta^3\text{-allyl})(bpy)(NSC)]$ in PrCN (Fig. 17) features a ν(CN) band at 2079 cm^{-1} and ν(CO) bands at 1950 and 1868 cm^{-1}. Upon the reduction, the new ν(CN) band rising at 2056 cm^{-1} corresponds to free NCS^-, being accompanied by ν(CO) bands resulting from multiple species. Importantly, the sharp ν(CO) band at 1892 cm^{-1} and broad ν(CO) band at 1775 cm^{-1} indicate that also the $[Mo(CO)_2(\eta^3\text{-allyl})(bpy)]_2$ dimer is formed on the initial reduction at room temperature, as seen in THF (Equations (1)–(4); Table 3). A second sharp ν(CO) band of an unassigned product is observed at 1906 cm^{-1}. UV–Vis spectroelectrochemistry (Fig. 18) shows the bands of the parent complex at 351 and 478 nm

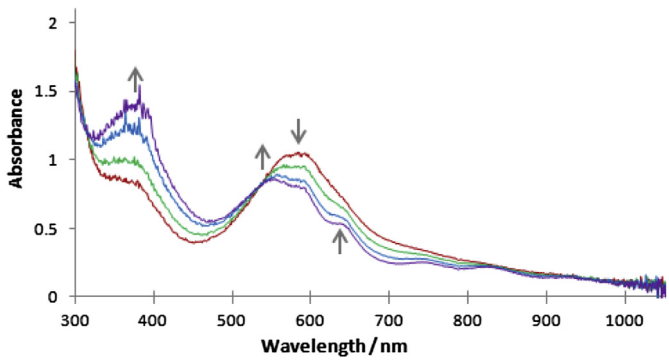

Fig. 15. UV–Vis spectroelectrochemistry showing the reduction of $[Mo(CO)_2(\eta^3\text{-allyl})(bpy)]_2$ (↓) to $[Mo(CO)_2(\eta^3\text{-allyl})(bpy)]^-$ (↑) in the THF/Bu_4NPF_6 electrolyte, within an OTTLE cell at room temperature.

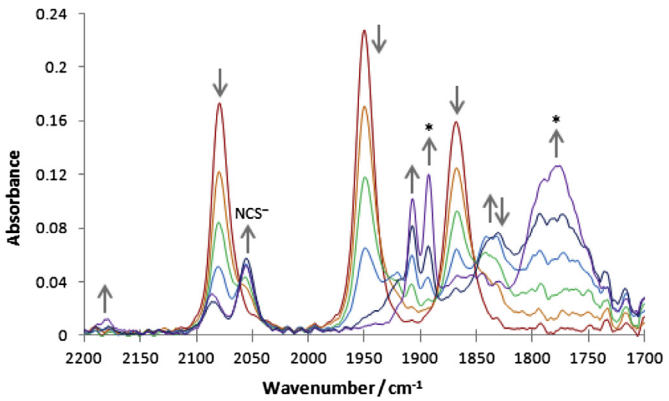

Fig. 17. Infrared spectroelectrochemistry of $[Mo(CO)_2(\eta^3\text{-allyl})(bpy)(NCS)]$ (↓) in the PrCN/Bu_4NPF_6 electrolyte, showing initial reduction and formation of $[Mo(CO)_2(\eta^3\text{-allyl})(bpy)]_2$ (↑ with asterisk) within an OTTLE cell at room temperature.

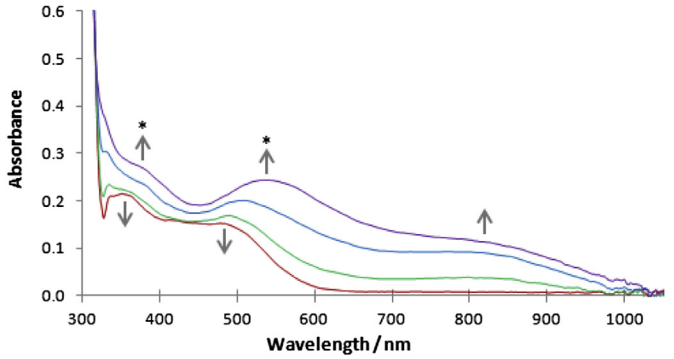

Fig. 18. UV–Vis spectroelectrochemistry of [Mo(CO)$_2$(η^3-allyl)(bpy)(NCS)] (↓) in the PrCN/Bu$_4$NPF$_6$ electrolyte, showing the initial reduction of the parent complex and formation of [Mo(CO)$_2$(η^3-allyl)(bpy)]$_2$ (↑ with asterisk) within an OTTLE cell at room temperature. The broad absorption band at 810 nm belongs to an unassigned reduction product.

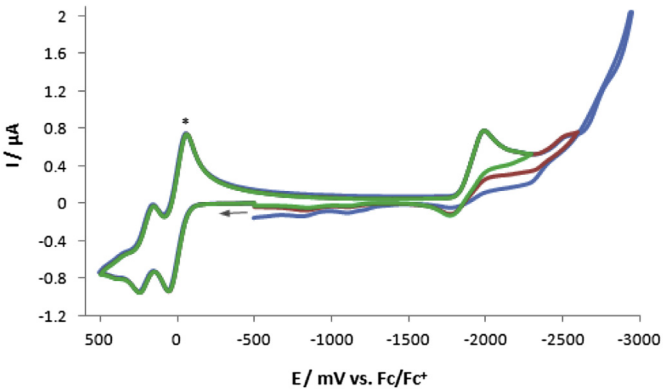

Fig. 19. Cyclic voltammogram of [Mo(CO)$_2$(η^3-allyl)(bpy)(NCS)] in the CO_2 saturated THF/Bu$_4$NPF$_6$ electrolyte at room temperature recorded at a scan rate of 100 mV s^{-1}. The Fc/Fc$^+$ standard couple is marked with asterisk. Cf. Fig. 2 for differences when CO_2 is absent.

are replaced by two bands at 371 and 538 nm, similar to those observed for [Mo(CO)$_2$(η^3-allyl)(bpy)]$_2$ in less polar THF (369, 581 nm). A new broad absorption broad arises at 810 nm. The ν(CO) band at 1906 cm^{-1} and the electronic absorption at 810 nm, both not observed in THF, are tentatively assigned to a different dimeric product, with further ν(CO) bands within the broad band at 1775 cm^{-1}. In addition, the small band at 2179 cm^{-1} points to PrCN coordination in a secondary reduction product [38].

Continued controlled-potential reduction of [Mo(CO)$_2$(η^3-allyl)(bpy)]$_2$ taking place in parallel with the other (dimeric?) species leads to another set of unassigned ν(CO) bands at 1910, 1882, 1835 and 1762 cm^{-1}, not belonging to [Mo(CO)$_2$(η^3-allyl)(bpy)(PrCN)]$^-$ or [Mo(CO)$_2$(η^3-allyl)(bpy)]$^-$. The corresponding UV–Vis spectra shows a typical bifurcated absorption band at 503 and 529 nm belonging to the [bpy$^{\bullet-}$] ligand. In order to avoid extensive speculative assignment, the reduction path in PrCN will be investigated in the near future in more detail using other methods such as EPR spectroscopy, applied to several derivatives of parent [Mo(CO)$_2$(η^3-allyl)(bpy)(NCS)] over a wider temperature range.

Overall, the reduction path documented for [Mo(CO)$_2$(η^3-allyl)(bpy)(NCS)] at room temperature closely resembles that of [Mn(CO)$_3$(bpy)X] [19,20], with the loss of the NCS$^-$ ligand from unstable [Mo(CO)$_2$(η^3-allyl)(bpy$^{\bullet-}$)(NCS)]$^-$ resulting in the eventual formation of the [Mo(CO)$_2$(η^3-allyl)(bpy)]$_2$ dimer from the reaction of [Mo(CO)$_2$(η^3-allyl)(bpy)]$^-$ with the parent complex in both THF and PrCN. At low temperature in PrCN, the cathodic behaviour of the [Mo(CO)$_2$(η^3-allyl)(bpy)(NCS)] complex more closely resembles that of [Re(CO)$_3$(bpy)X] [7] with formation of a six-coordinate solvento anion, [Mo(CO)$_2$(η^3-allyl)(bpy)(PrCN)]$^-$.

3.8. Cyclic voltammetry of [Mo(CO)$_2$(η^3-allyl)(bpy)(NCS)] in a CO_2-saturated THF electrolyte

The cyclic voltammogram of [Mo(CO)$_2$(η^3-allyl)(bpy)(NCS)] was also recorded in dry THF saturated with CO_2 under normal atmospheric pressure (Fig. 19), in order to probe the ability of the complex to electrocatalyse CO_2 reduction.

No change is seen to the irreversible cathodic wave, R1, at $E_{p,c} = -1.99$ V, but the intensity of the O1′ anodic counter peak at $E_{p,a} = -1.77$ V has decreased upon addition of CO_2. This behaviour indicates a possible interaction of CO_2 with the five-coordinate anion, [Mo(CO)$_2$(η^3-allyl)(bpy)]$^-$, formed at $E_{p,c} = -1.99$ V. Further small anodic waves are observed at $E_{p,a} = -1.10$ V and −0.83 V. A high (catalytic) current is seen following the reduction of the [Mo(CO)$_2$(η^3-allyl)(bpy)]$_2$ dimer at $E_{p,c} = -2.52$ V, resulting in the formation of [Mo(CO)$_2$(η^3-allyl)(bpy)]$^-$.

3.9. Spectroelectrochemistry of [Mo(CO)$_2$(η^3-allyl)(bpy)(NCS)]: reduction in CO_2-saturated THF electrolyte

IR monitoring of the reduction of [Mo(CO)$_2$(η^3-allyl)(bpy)(NCS)] in CO_2-saturated THF shows the initial appearance of ν(CO) bands at 1916 and 1818 cm^{-1} (Fig. 20). The ν(CN) band shifts to 2053 cm^{-1} as the NCS$^-$ ligand dissociates. Small bands are also observed forming at 1717 cm^{-1} (the stretching mode of coordinated O_2CH^-), and at 1890, 1634 and 1580 cm^{-1}. Notably, the intensity of the $^{13}CO_2$ satellite peak at 2272 cm^{-1} does not change significantly. The shift of the ν(CO) bands (35–53 cm^{-1}) is significantly smaller than would be expected for the formation of an anionic species. Therefore, this species is likely to be the neutral formate complex, [Mo(CO)$_2$(η^3-allyl)(bpy)(O_2CH)], reducible at a more negative cathodic potential than the parent NCS-complex.

Upon further reduction (Fig. 21), a new species was observed with ν(CO) bands at 1889 and 1762 cm^{-1}, possibly relating to the dimer [Mo(CO)$_2$(η^3-allyl)(bpy)]$_2$ (Table 3). The intensity of the $^{13}CO_2$ band significantly decreased (Fig. 21, inset), and new ν(C=O) bands were seen rising rapidly at 1674 and 1641 cm^{-1}, belonging to

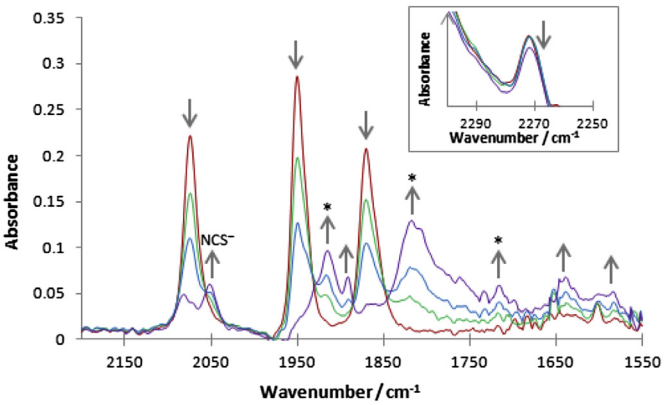

Fig. 20. Infrared spectroelectrochemistry of [Mo(CO)$_2$(η^3-allyl)(bpy)(NCS)] (↓) in the CO_2-saturated THF/Bu$_4$NPF$_6$ electrolyte within an OTTLE cell. Inset: Decay of the $^{13}CO_2$ satellite peak. The three product bands (↑) labelled with asterisk belong likely to [Mo(CO)$_2$(η^3-allyl)(bpy)(O_2CH)].

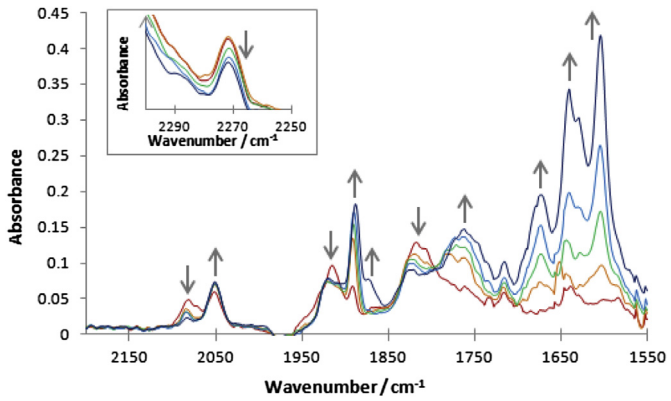

Fig. 21. Infrared spectroelectrochemistry of $[Mo(CO)_2(\eta^3\text{-allyl})(bpy)(NCS)]$ (↓) in the CO_2 saturated THF/Bu_4NPF_6 electrolyte within an OTTLE cell. For the preceding non-catalytic process see Fig. 20. Inset: decay of the $^{13}CO_2$ satellite peak.

HCO_3^- that typically accompanies the CO production; the third intense ν(C═O) band at 1605 cm^{-1} corresponds to the catalytic production of free formate. In addition, small bubbles were developing at the working electrode minigrid, indicating the formation of CO. The gas development limited the scope of the monitoring of the electrocatalytic reaction to the initial 10 min.

Comparison of the cyclic voltammetry and IR spectroelectrochemistry of $[Mo(CO)_2(\eta^3\text{-allyl})(bpy)(NCS)]$ in THF in the presence of CO_2 shows that upon the initial reduction, a neutral formate complex $[Mo(CO)_2(\eta^3\text{-allyl})(bpy)(O_2CH)]$, is produced which must itself be reduced for the catalytic reduction of CO_2 to occur. An identical electrocatalytic behaviour has recently been observed [39] for $[Mn(CO)_3(^i\text{Pr-DAB})]^-$ (^{i}Pr-DAB = *N*,*N*′-di-isopropyl-1,4-diazabuta-1,3-diene) in the CO_2-saturated THF electrolyte, which exhibits a very similar reduction path [20].

4. Conclusions

The redox behaviour of $[Mo(CO)_2(\eta^3\text{-allyl})(bpy)(NCS)]$ was studied using both cyclic voltammetry and in situ UV–Vis/IR spectroelectrochemistry in THF and PrCN at 293 K and in PrCN at 200–183 K. The previously unreported $[Mo(CO)_2(\eta^3\text{-allyl})(2,6\text{-xylyl-BIAN})(NCS)]$ complex was synthesised and characterised by NMR, IR and UV–Vis spectroscopy, and X-ray crystallography. The extended π-aromatic system of the strongly π-accepting 2,6-xylyl-BIAN ligand stabilises the six-coordinate radical anion $[Mo(CO)_2(\eta^3\text{-allyl})(2,6\text{-xylyl-BIAN}^{\bullet-})(NCS)]^-$ formed on the initial reduction, and this assisted in the assignment of the products formed by reduction of $[Mo(CO)_2(\eta^3\text{-allyl})(bpy)(NCS)]$ and in the determination of the reduction path.

The reduction of $[Mo(CO)_2(\eta^3\text{-allyl})(bpy)(NCS)]$ in THF resulted in dissociation of the spectator NCS^- ligand and concomitant reduction of $[Mo(CO)_2(\eta^3\text{-allyl})(bpy^{\bullet-})]$ to give the five-coordinate anion $[Mo(CO)_2(\eta^3\text{-allyl})(bpy)]^-$, that reacts with the yet unreduced parent complex to produce the dimer $[Mo(CO)_2(\eta^3\text{-allyl})(bpy)]_2$. $[Mo(CO)_2(\eta^3\text{-allyl})(bpy)]^-$ is observed following the reduction of $[Mo(CO)_2(\eta^3\text{-allyl})(bpy)]_2$ in THF, but in PrCN this cathodic step is significantly more complex. Importantly, it has been shown for the first time that $[Mo(CO)_2(\eta^3\text{-allyl})(bpy)]^-$ is capable of catalysing the reduction of CO_2 to CO and formate via formation and subsequent reduction of $[Mo(CO)_2(\eta^3\text{-allyl})(bpy)(O_2CH)]$. Further investigation of this family of electrocatalysts, closely related to $[Mn(CO)_3(R\text{-bpy})(halide)]$ [9,10,20], has been in progress.

Acknowledgements

The authors thank the University of Reading for provision of the Chemical Analysis Facility (the CAF lab). FH is also grateful to the University of Reading for a start-up grant covering this project. Mr Henk Luyten (Purmerend, The Netherlands) is thanked for the maintenance of the spectroelectrochemical cells in the Reading Spectroelectrochemistry Laboratory (RSL) and Mr Nick Spencer for assistance in collection of the single-crystal data in the CAF lab. Dr. Qiang Zeng (University of Reading, RSL) kindly helped with the preparation of the experimental setup for spectroelectrochemistry at low temperatures.

Appendix A. Supplementary material

CCDC 967234 (**1**) contains the supplementary crystallographic data for this paper. These data can be obtained free of charge from The Cambridge Crystallographic Data Centre via www.ccdc.cam.ac.uk/data_request/cif.

Appendix B. Supplementary data

Supplementary data related to this article can be found at http://dx.doi.org/10.1016/j.jorganchem.2014.01.015.

References

[1] J.M. Savéant, Chem. Rev. 108 (2008) 2348–2378.
[2] E.E. Benson, C.P. Kubiak, A.J. Sathrum, J.M. Smieja, Chem. Soc. Rev. 38 (2009) 89–99.
[3] A.J. Morris, G.J. Meyer, E. Fujita, Acc. Chem. Res. 42 (2009) 1983–1994.
[4] C. Finn, S. Schnittger, L.J. Yellowlees, J.B. Love, Chem. Commun. 48 (2012) 1392–1399.
[5] C.D. Windle, R.N. Perutz, Coord. Chem. Rev. 256 (2012) 2562–2570.
[6] B.P. Sullivan, C.M. Bolinger, D. Conrad, W.J. Vining, T.J. Meyer, J. Chem. Soc. Chem. Commun. (1985) 1414–1415.
[7] F.P.A. Johnson, M.W. George, F. Hartl, J.J. Turner, Organometallics 15 (1996) 3374–3387.
[8] H. Takeda, O. Ishitani, Coord. Chem. Rev. 254 (2010) 346–354.
[9] M. Bourrez, F. Molton, S. Chardon-Noblat, A. Deronzier, Angew. Chem. Int. Ed. 50 (2011) 9903–9906.
[10] J.M. Smieja, M.D. Sampson, K.A. Grice, E.E. Benson, J.D. Froehlich, C.P. Kubiak, Inorg. Chem. 52 (2013) 2484–2491.
[11] J. Tory, B. Setterfield-Price, J. McDouall, R.A.W. Dryfe, F. Hartl, manuscript in preparation.
[12] J.W. Faller, D.A. Haitko, R.D. Adams, D.F. Chodosh, J. Am. Chem. Soc. 101 (1979) 865–876.
[13] J.R. Ascenso, C.G. de Azevedo, M.J. Calhorda, M. Carrondo, P. Costa, A.R. Dias, M.G.B. Drew, V. Felix, A.M. Galvao, C.C. Romao, J. Organomet. Chem. 632 (2001) 197–208.
[14] F.-C. Liu, P.-S. Yang, C.-Y. Chen, G.-H. Lee, S.-M. Peng, J. Organomet. Chem. 693 (2008) 537–545.
[15] J. Perez, V. Riera, A. Rodriguez, R. Lopez, T.L. Sordo, S. Garcia-Granda, E. Garcia-Rodriguez, A. Galindo, Organometallics 22 (2003) 1540–1545.
[16] M.D. Curtis, O. Eisenstein, Organometallics 3 (1984) 887–895.
[17] B.J. Brisdon, K.A. Conner, R.A. Walton, Organometallics 2 (1983) 1159–1163.
[18] B.J. Brisdon, S.K. Enger, M.J. Weaver, R.A. Walton, Inorg. Chem. 26 (1987) 3340–3344.
[19] F. Hartl, B.D. Rossenaar, G.J. Stor, D.J. Stufkens, Recl. Trav. Chim. Pays-Bas 114 (1995) 565–570.
[20] B.D. Rossenaar, F. Hartl, D.J. Stufkens, C. Amatore, E. Maisonhaute, J.N. Verpeaux, Organometallics 16 (1997) 4675–4685.
[21] R. van Asselt, C.J. Elsevier, W.J.J. Smeets, A.L. Spek, R. Benedix, Recl. Trav. Chim. Pays-Bas 113 (1994) 88–98.
[22] J.W. Goodyear, C.W. Hemingway, R.W. Harrington, M.R. Wiseman, B.J. Brisdon, J. Organomet. Chem. 664 (2002) 176–181.
[23] C.G. Hull, M.H.B. Stiddard, J. Organomet. Chem. 9 (1967) 519–525.
[24] A.J. Graham, R.H. Fenn, J. Organomet. Chem. 17 (1969) 405–422.
[25] AgilentTechnologies, Xcalibur/SuperNova CCD System, CrysAlisPro Software System, Version 1.171.36.21, Agilent Technologies UK Ltd., Oxford, UK, 2012.
[26] L. Palatinus, G. Chapius, J. Appl. Cryst. 40 (2007) 786–790.
[27] P.W. Betteridge, J.R. Carruthers, R.I. Cooper, C.K. Prout, D.J. Watkin, J. Appl. Cryst. 36 (2003) 1487.
[28] P. van der Sluis, A.L. Spek, Acta Crystallogr. A46 (1990) 194–201.
[29] M. Krejčík, M. Danek, F. Hartl, J. Electroanal. Chem. 317 (1991) 179–187.

[30] F. Hartl, H. Luyten, H.A. Nieuwenhuis, G.C. Schoemaker, Appl. Spectrosc. 48 (1994) 1522–1528.
[31] T. Mahabiersing, H. Luyten, R.C. Nieuwendam, F. Hartl, Collect. Czech. Chem. Commun. 68 (2003) 1687–1709.
[32] A. Klein, W. Kaim, Organometallics 14 (1995) 1176–1186.
[33] T. Turki, T. Guerfel, F. Bouachir, Polyhedron 28 (2009) 569–573.
[34] K. Ohta, K. Tominaga, Chem. Phys. Lett. 429 (2006) 136–140.
[35] G.J. Stor, F. Hartl, J.W.M. van Outersterp, D.J. Stufkens, Organometallics 14 (1995) 1115–1131.
[36] F. Hartl, M.P. Aarnts, H.A. Nieuwenhuis, J. van Slageren, Coord. Chem. Rev. 230 (2002) 107–125.
[37] F. Hartl, P. Rosa, L. Ricard, P. Le Floch, S. Záliš, Coord. Chem. Rev. 251 (2007) 557–576.
[38] F. Hartl, A.K. Renfrew, F. Lafolet, T. Mahabiersing, M.J. Calhorda, S. Chardon-Noblat, M. Haukka, A. Deronzier, Inorg. Chem. 48 (2009) 8233–8244.
[39] J. Tory, Q. Zeng, F. Hartl, unpublished results, Reading, 2012.

Please cite this article in press as: J. Tory, et al., Journal of Organometallic Chemistry (2014), http://dx.doi.org/10.1016/j.jorganchem.2014.01.015